Available online at www.sciencedirect.com
ScienceDirect
Trans. Nonferrous Met. Soc. China 33(2023) 3503−3513
Transactions of Nonferrous Metals Society of China
www.tnmsc.cn

Interface-coupled $PbSO_4$ dissolution and PbS precipitation and its effect on sulfidization flotation of anglesite

Jia-lei LI[1], Guang-li LI[2], Zhi-cheng LIU[2], Shuai NING[1,3], Rui-zeng LIU[1, 3]

1. Faculty of Land Resources Engineering, Kunming University of Science and Technology, Kunming 650093, China;
2. Yunnan Chihong Zn & Ge Co., Ltd., Qujing 655000, China;
3. Yunnan Key Laboratory of Green Separation and Enrichment of Strategic Mineral Resources, Kunming 650093, China

Received 13 April 2022; accepted 30 September 2022

Abstract: Anglesite sulfidization mechanism was systematically investigated using flotation tests, X-ray photoelectron spectroscopy (XPS), field-emission scanning electron microscopy (FESEM), Raman spectroscopy, and ultraviolet−visible diffuse reflectance spectroscopy (UV−Vis DRS). The activation effect of sodium sulfide on anglesite flotation was demonstrated by the flotation tests; however, sodium sulfide concentration must be properly controlled to avoid excessive sulfide ions causing flotation depression. The results of XPS, Raman, and UV−Vis DRS revealed that $PbSO_4$ was replaced by PbS during anglesite treatment with a sodium sulfide aqueous solution. FESEM imaging shows the dissolution of $PbSO_4$ and the precipitation of PbS nanoparticles during sulfidization. Thus, it can be suggested that the reaction of anglesite with a sodium sulfide aqueous solution proceeds via an interface-coupled dissolution–precipitation mechanism: upon contact with a sodium sulfide aqueous solution, anglesite dissolution releases Pb^{2+} and SO_4^{2-} into the fluid boundary layer, which becomes oversaturated with respect to PbS phase; then the PbS nanoparticles nucleate and grow on the surface of anglesite. The PbS nanoparticles grown on anglesite can improve the floatability of anglesite.
Key words: anglesite; $PbSO_4$; PbS; sulfidization mechanism; flotation; dissolution; precipitation

1 Introduction

Anglesite ($PbSO_4$) is a secondary lead mineral, derived from the weathering of lead sulfide mineral. In nature, anglesite is replaced by cerussite ($PbCO_3$) when it comes into contact with CO_2-rich fluids [1]. Therefore, cerussite and anglesite are the most and second-most important non-sulfide lead minerals (popularly called oxidized minerals), respectively. However, anglesite can also be the most abundant non-sulfide lead mineral in the weathering zones of some ore deposits, such as the Kuh-e-Surmeh Deposit in Fars, Iran [2], and the Pb−Zn−Cd Fule Deposit in Yunnan Province, China [3]. Anglesite is also the main Pb-bearing material in hydrometallurgical zinc-leaching residues [4−6].

Sulfidization flotation is a common and low-cost method for recovering oxidized minerals of base metals [7]. Sulfidization converts the surfaces of oxidized minerals to more hydrophobic sulfide compounds that are suitable for xanthate flotation, which is a critical stage in this flotation process. Thus, the sulfidization mechanisms of oxidized minerals have been extensively studied [8,9]. Two classic interpretations have been proposed on the sulfidization mechanism: (1) chemisorption of sulfide ions on the surfaces of oxidized minerals, and (2) substitution of sulfide ions in oxidized mineral crystal lattice via solid-state diffusion, also known as “ion exchange” of sulfide ions with the anions of the mineral lattice [10,11]. By definition,

Corresponding author: Rui-zeng LIU, Tel: +86-871-65915598, E-mail: liuruizeng@126.com
DOI: 10.1016/S1003-6326(23)66350-2

chemisorption produces a monolayer surface complex rather than a new phase. Nevertheless, recent morphology, textural, and kinetic evidences have shown that the sulfidization product of oxidized minerals is a solid multilayer rather than a monolayer (i.e. a new solid phase) [12−17]. The ion exchange mechanism involves the preservation of the crystal structure and the interdiffusion of ions through the solid. However, the oxidized minerals usually have different crystal structures with their corresponding sulfidization products; in addition, the diffusion of ions in solids needs to overcome the energy barrier to motion, which is kinetically unfavorable under ambient conditions [18,19]. As a result, the sulfidization of oxidized minerals is more likely to occur via a mechanism that has not yet been discussed in the field of flotation research.

In geoscience and environmental science, interface-coupled dissolution–precipitation (ICDP) rather than solid-state diffusion has been acknowledged as a universal mechanism for the solid−solid phase transformation during solid−aqueous solution interaction [18−21]. According to the ICDP mechanism, an aqueous solution will induce the dissolution of an insoluble or even an extremely insoluble phase, generating an interfacial boundary layer of the aqueous solution that may be oversaturated with respect to a more stable solid phase. Then, the nucleation and growth of the new phase on the surface of the parent phase may occur and thereby promote the dissolution of the parent phase, which in turn accelerates the growth of the product phase. That is, in the presence of an aqueous solution, the dissolution of a less stable phase and the precipitation of a more stable phase coupling occur at a solid–aqueous solution interface [19].

Sulfidization flotation processes have been used for decades to recover anglesite from lead oxide ores, mixed sulfide−oxide lead ores, zinc-leaching residues, and sintering dust [4,6,22,23]. However, to the best of our knowledge, little research has been conducted into the sulfidization mechanism in anglesite flotation. Information gaps still exist on the chemical states, elemental compositions and morphologies, and so on, of the surfaces of the sulfidized anglesite. This study aimed to examine the effect of sulfidization on the floatability of anglesite, and investigate whether anglesite sulfidization occurs via an ICDP mechanism. These purposes would be achieved by conducting flotation tests, X-ray photoelectron spectroscopy (XPS), field-emission scanning electron microscopy (FESEM), Raman spectroscopy, and ultraviolet−visible diffuse reflectance spectroscopy (UV−Vis DRS).

2 Experimental

2.1 Materials

Analytical-grade $PbSO_4$ particles (purity > 98% on a metal basis) were purchased from Tianjin Guangfu Fine Chemical Research Institute, China. The particles were dispersed and dry-screened to obtain size fractions (≤ 74 μm) for use in this study. Analytical-grade PbS particles (purity > 99.9% on the metal basis, Macklin) were used as a reference sample in the UV−Vis DRS analyses. The X-ray diffraction (XRD) patterns of $PbSO_4$ (Fig. S1 in Supporting Information) and PbS (Fig. S2) samples matched the standard patterns for anglesite $PbSO_4$ (JCPDS No. 36-1461) and galena PbS (JCPDS No. 05-0592), respectively.

Analytical-grade sodium sulfide ($Na_2S·9H_2O$) was used as a sulfidizing agent, and analytical-grade methyl isobutyl methanol (MIBC) was used as a foaming agent. Analytical-grade sulfuric acid or sodium hydroxide was used for pH regulation. Na_2S, MIBC, H_2SO_4, and NaOH were obtained from Sinopharm Chemical Reagent Co., Ltd. Industry-grade sodium amyl xanthate (NaAX) obtained from Hunan Mingzhu Flotation Reagents Co., Ltd., China, was used as a collector.

Deionized water (resistivity >18.2 MΩ·cm) prepared by the Hitech laboratory water purification system was used in this study.

2.2 Flotation tests

Flotation tests were carried out in a 40 mL flotation cell. For each test, a 3.0 g anglesite sample and a given amount of deionized water were put in the flotation cell to prepare a pulp suspension. After stirring for 1 min, a sodium sulfide aqueous solution with a specific concentration was dosed into the pulp to react for 3 min. Then, when the pulp pH was adjusted to a specific value using NaOH or H_2SO_4 solutions, the pulp was conditioned with NaAX and MIBC for 3 min. After flotation for 3 min, the floating and sunken products were dried and weighed to calculate the recovery. Each test

was repeated three times or more, and their average value was taken as the final result; in addition, the standard deviation was plotted as an error bar.

2.3 Characterization

The samples for characterization underwent the same sulfidization process as the flotation test samples. After sulfidization, the samples were washed and dried. Before measurements, the samples were stored in vacuum-sealed bags to minimize oxidation.

The elemental compositions and chemical states on the raw and sulfidized anglesite surfaces were examined with an X-ray photoelectron spectrometer (PHI5000 Versaprobe III, Ulvac-Phi, Japan). The operating parameters were as follows: Al K_α radiation, working voltage 15 kV, takeoff angle 45°, and passing energy 69 eV; the obtained data were corrected using the adventitious carbon C 1s peak at 284.80 eV, and then were analyzed using MultiPak software. The phase composition of the outer layers of anglesite particles before and after sulfidization was determined using Raman spectroscopy (532 nm line of a He−Ne laser, Horiba Evolution spectrophotometer, HORIBA Scientific, France) and DRS (UV−3600 spectrophotometer, Shimadzu, Japan). The referenced Raman spectra of anglesite $PbSO_4$ and galena PbS were obtained from the RRUFF Project (https://rruff.info). Surface morphologies of the raw and sulfidized anglesite particles were imaged by a Zeiss Sigma 300 field-emission electron microscope (Zeiss, Germany); before imaging, the samples were coated with platinum to improve their surface conductivity.

3 Results and discussion

3.1 Flotation test results

Figure 1 shows the effect of pulp pH on raw and sulfidized anglesite flotation. The flotation recoveries of raw and sulfidized anglesite increased slightly with increasing pH until approximately 7. At pH ~7, the flotation recoveries of raw and sulfidized anglesite were 33.3% and 68.0%, respectively. When pulp pH > 7, the flotation recoveries of raw and sulfidized anglesite decreased sharply; at pH 9.58, flotation recoveries for raw and sulfidized anglesite were only approximately 5.0%. The results showed that anglesite flotation is adversely affected under higher pH conditions, which may be attributed to the instability of anglesite under higher pH conditions [24]. Furthermore, it is apparent from Fig. 1 that recoveries of sulfidized anglesite were higher than those of raw anglesite at pH <8.5, which demonstrates the positive effect of sulfidization on anglesite flotation.

Figure 2 shows that the shape of the anglesite's flotation recovery vs sodium sulfide concentration presents an inverted U-shaped curve, which is consistent with those of other oxidized minerals, such as malachite [12], cerussite [13], azurite [25], and cuprite [26]. In Fig. 2, the anglesite recovery increased from 33.3% to 71.8% as sodium sulfide concentration increased from 0 to 1.5 m mol/L; however, once the sodium sulfide concentration exceeded the optimal value, anglesite flotation recovery declined. The results further showed the promotion of sulfidization on anglesite flotation; however, the concentration of sodium sulfide has to be strictly controlled to avoid excessive sulfide ions depressing the flotation.

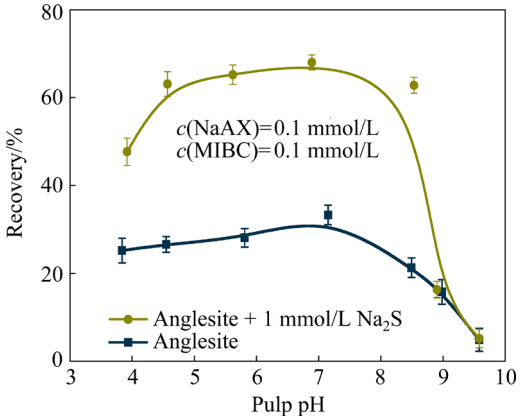

Fig. 1 Effect of pulp pH on anglesite flotation recovery with and without sodium sulfide

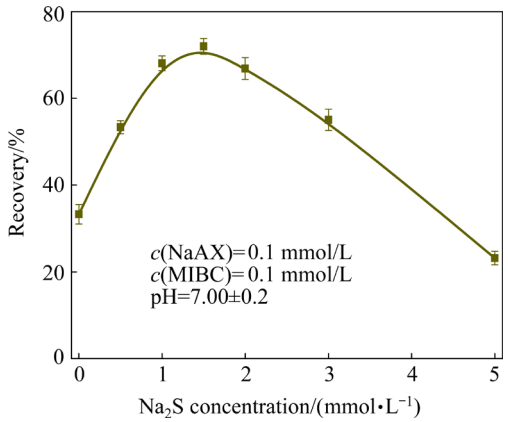

Fig. 2 Flotation recovery of anglesite vs sodium sulfide concentration

3.2 XPS spectra

In the XPS study, high-resolution spectra of Pb 4f and O 1s were used to analyze lead and oxygen, respectively. For sulfur, in general, stronger S 2p spectra were used instead of S 2s spectra. However, the S 2p peak region overlaps the energy loss peak of the Pb 4f line, interfering with concentration calculations and peak recognition [14]. Considering this, this study is dependent on the S 2s spectra which also show a larger range of chemical shifts. The S 2p spectra are used as an ancillary reference.

Figures 3(a) and (b) show the S 2s and S 2p spectra of the raw and sulfidized anglesite, respectively. For raw anglesite (Sample 1, without Na_2S solution treatment), only one S 2s peak appeared at 232.50 eV (Fig. 3(a)), and one S 2p spin-orbit doublet consisting of S $2p_{3/2}$ peak at 168.30 eV and S $2p_{1/2}$ peak at 169.48 eV was observed (Fig. 3(b)), both of which agreed with sulfur in $PbSO_4$ in NIST XPS database [27]. In addition, as expected, a not very sharp peak appeared at 163.70 eV in the S 2p spectrum, which was attributed to the energy loss peak of the Pb 4f line. After sulfidization (Samples 2 and 3 treated with 1.5 and 5.0 mmol/L Na_2S solution, respectively), new S 2s peaks emerged at (225.25±0.07) eV (Fig. 3(a)), and new S $2p_{3/2}$ and S $2p_{1/2}$ doublets appeared at binding energies of 160.80 and 161.98 eV, respectively (Fig. 3(b)), both of which could be assigned to sulfur in PbS [27]. Figure 3 also shows that with increasing the concentration of sodium sulfide, the intensity of the S 2s and S 2p peaks corresponding to $PbSO_4$ decreased while those corresponding to PbS increased.

Figure 4(a) presents the Pb 4f spectra of the raw and sulfidized anglesite samples. In the spectrum of raw anglesite (Sample 1), the peaks at 139.28 and 144.14 eV are respectively attributed to the Pb $4f_{7/2}$ and Pb $4f_{5/2}$ spin-orbit doublets of $PbSO_4$, respectively [27]. After sulfidization (Samples 2 and 3), two new Pb $4f_{7/2}$ and Pb $4f_{5/2}$ spin-orbit doublets emerged at binding energies of 137.60 and 142.46 eV, respectively, which are ascribed to PbS [27]. Similarly, with increasing the concentration of sodium sulfide, the doublets corresponding to $PbSO_4$ decreased while those corresponding to PbS increased.

The O 1s spectra of the raw and sulfidized anglesite are plotted in Fig. 4(b). All of O 1s peaks were at 531.50 eV and could be attributed to O in $PbSO_4$ [27]. Furthermore, the intensity of O 1s peaks decreased with increasing sodium sulfide concentration.

To more clearly show surface changes before and after anglesite sulfidization, semi-quantitative

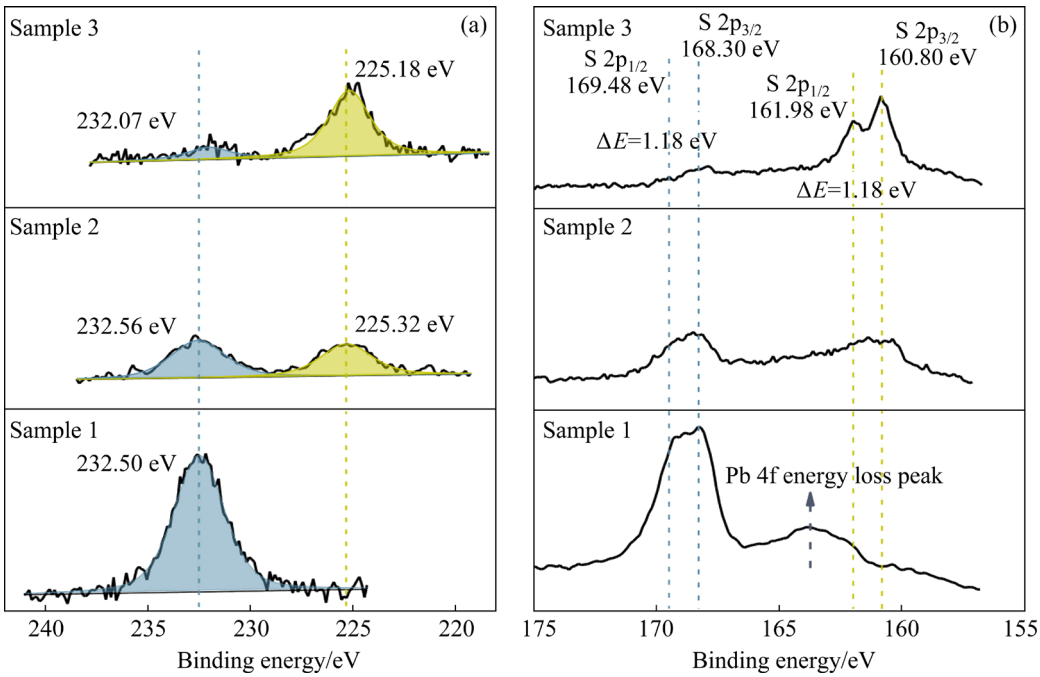

Fig. 3 High-resolution XPS spectra of S 2s (a) and S 2p (b) for anglesite treatment with and without sodium sulfide solutions

analyses of element content on raw and sulfidized anglesite surfaces were carried out. Table S1 in Supporting Information shows the element content and atomic ratio of the raw anglesite surfaces calculated based on the Pb 4f, S 2p, and O 1s spectra. As shown in Table S1, the contents of Pb, S, and O were 14.24 at.%, 32.95 at.%, and 52.81 at.%, respectively, and the Pb/S/O molar ratio was 1:2.31:3.70, both of which were significantly different from that expected for $PbSO_4$, demonstrating the negative effect caused by the energy loss peak of the Pb 4f line. Thus, the element contents were calculated based on the Pb 4f, S 2s, and O 1s spectra, which are listed in Table 1. Table 1 shows that the contents of Pb, S, and O for the raw anglesite were 16.86 at.%, 18.99 at.%, and 64.14 at.%, respectively, and the Pb/S/O molar ratio was 1:1.13:3.80, both of which were close to the theoretical values for $PbSO_4$. As seen in Table 1, with increasing sodium sulfide concentration, the total contents of Pb and S increased while that of O decreased. After sulfidization, the total contents of Pb and S increased because PbS had higher Pb and S contents than $PbSO_4$. Interestingly, the S/Pb molar ratio remained at approximately 1, indicating that $PbSO_4$ was replaced by PbS at a S/Pb molar ratio of about 1 during anglesite sulfidization.

3.3 Raman spectra and DRS results

Typically, X-ray diffraction (XRD) analysis is the most powerful technique for phase composition identification. However, under the flotation-related circumstances, the sulfidization products of oxidized minerals cannot be identified because XRD analysis is not sensitive to the low-content phases [12,13]. In contrast, Raman spectroscopy and DRS have advantages in examining the phase compositions on the surface of solids [15,28,29].

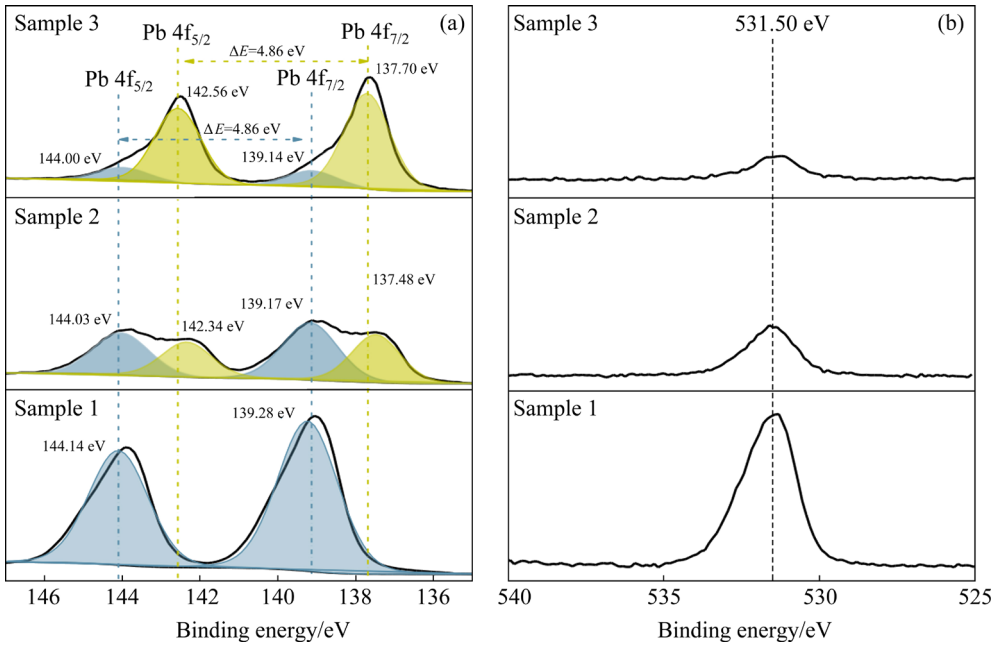

Fig. 4 High-resolution XPS spectra of Pb 4f (a) and O 1s (b) for anglesite with and without sodium sulfide solution treatment

Table 1 Element contents and molar ratios of raw and sulfidized anglesite samples calculated based on Pb 4f, S 2 s and O 1s spectra

Sample No.	Content/at.%							S/Pb molar ratio	O/Pb molar ratio
	Total Pb	Pb in $PbSO_4$	Pb in PbS	Total S	S in $PbSO_4$	S in PbS	O		
1	16.86	16.86	0.00	18.99	18.99	0.00	64.14	1.13	3.80
2	25.79	14.6	11.19	24.15	13.2	10.95	50.06	0.93	1.94
3	32.20	5.03	27.17	30.60	5.62	24.98	37.79	0.95	1.17

Figure 5(a) shows the optical photographs and optical micrographs corresponding to Raman spectra of raw and sulfidized samples. The raw anglesite powder (Sample 1) was milky white to the naked eye but colorless and transparent under an optical microscope. After treatment with a 1.5 mmol/L sodium sulfide solution (Sample 2), the anglesite particles turned light brown, and the optical micrographs showed that some regions turned black, while some remained colorless and transparent. When sodium sulfide concentration was 5 mmol/L (Sample 3), the particles appeared black to the naked eye, and the optical microscopy image showed that the particles were reflective and metallic black, similar to galena PbS. These color changes are the most conspicuous evidence of the transformation from $PbSO_4$ to PbS.

As shown in Fig. 5(b), the measured spectrum of raw anglesite (Sample 1) is in good agreement with the referenced spectrum ($PbSO_4$, RRUFF ID: 050408) and published data [30]. In the measured Raman spectrum of raw anglesite, a strong peak at 978 cm^{-1} is attributed to the sulfate stretching vibration (v_1), peaks at 439 and 450 cm^{-1} to v_2 vibrational mode, peaks at 1060 and 1158 cm^{-1} to v_3 vibrational mode, and weak peaks at 607 and 642 cm^{-1} to v_4 vibrational mode [31]. However, peaks for PbS were not observed in the Raman spectra of the sulfidized anglesite (Samples 2 and 3), because PbS with a rock salt-type crystal structure shows no Raman active modes [32].

Figure 6 shows the UV−Vis DRS spectra of raw and sulfidized anglesite as well as the PbS reference sample. The raw anglesite showed strong absorption in the UV region (200−400 nm) but weak absorption in the visible light region; in addition, an absorption peak was observed at ~300 nm. Interestingly, the sulfidized anglesite showed light absorption characteristics similar to that of the PbS reference sample, further suggesting the formation of PbS on the surface of the sulfidized anglesite.

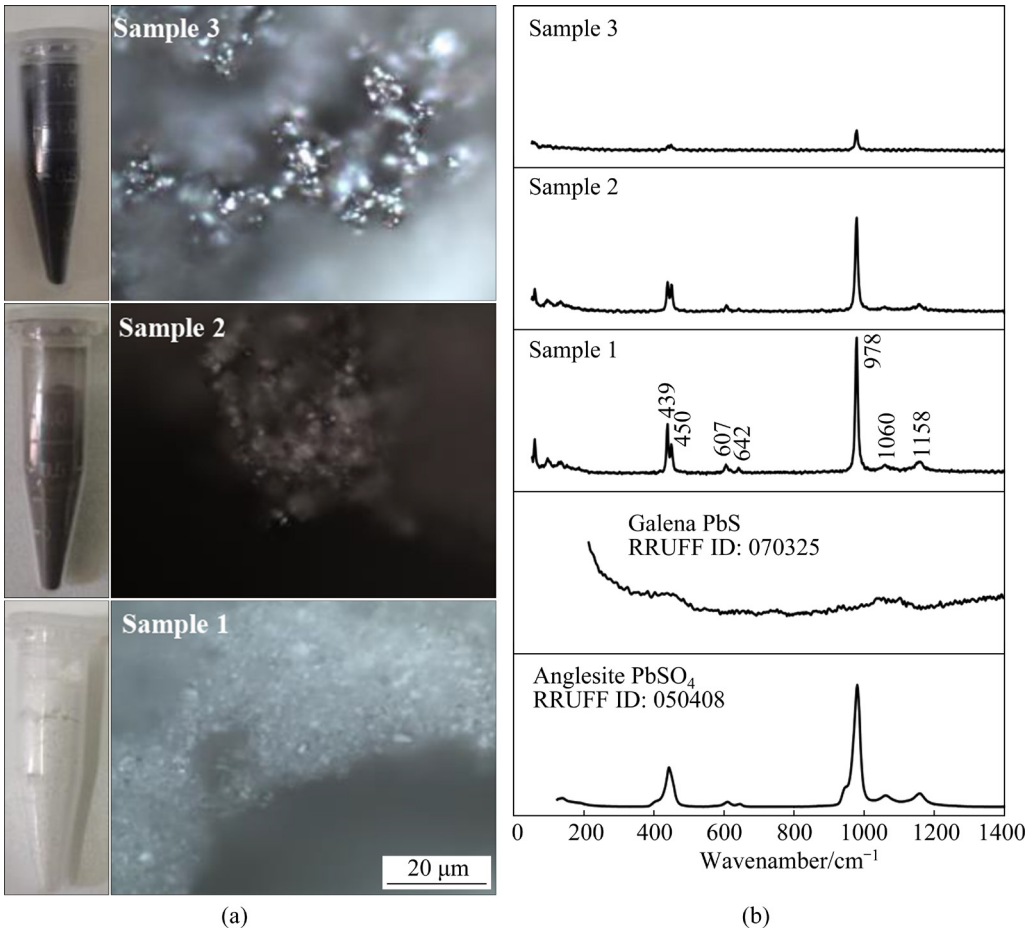

Fig. 5 Optical photographs (left) and optical micrographs (right) (a), and Raman spectra (b) corresponding to optical micrographs in (a)

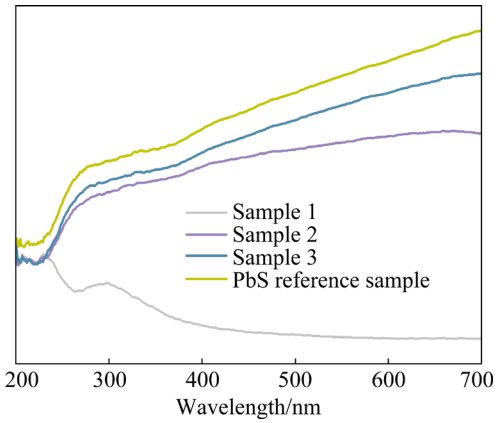

Fig. 6 UV−Vis DRS spectra of anglesite particles treated with different sodium sulfide concentrations and PbS reference sample

As shown in Fig. 5(b), the intensity of $PbSO_4$ of the Raman peaks decreased considerably with increasing sodium sulfide concentration. The sulfidized anglesite showed strong light absorption in the visible light region; therefore, the measured Raman signals were mostly from the surfaces of the samples [28]. Thus, the decrease in peak intensities suggested that the $PbSO_4$ content on the surfaces of the samples decreased with increasing sodium sulfide concentration. Consequently, the Raman and DRS spectra provided clear evidence of the replacement of $PbSO_4$ by PbS on the surface of anglesite during sulfidization.

3.4 FESEM observation

Figure 7 shows the FESEM images of the raw and sulfidized anglesite particles at different magnifications. At low magnifications (Figs. 7(a_1, b_1, c_1)), the sample particles were tabular, which was one of the common crystal morphologies of anglesite.

The anglesite crystal particles after treatment with deionized water showed geometrically regular edges and corners, and the surface was relatively smooth. However, considerable microcracks were observed under high magnification (Fig. 7(a_3)), which may be caused by platinum spraying before FESEM measurements. After treatment with sodium sulfide solutions, a larger number of nanoparticles with relatively uniform shapes and sizes grew on anglesite surfaces (Figs. 7(b) and (c)). Previous XPS, Raman, and DRS studies have demonstrated the formation of PbS on the surfaces of anglesite treated with sodium sulfide solution; thus, it can be considered that these nanoparticles were the sulfidization product of anglesite, namely

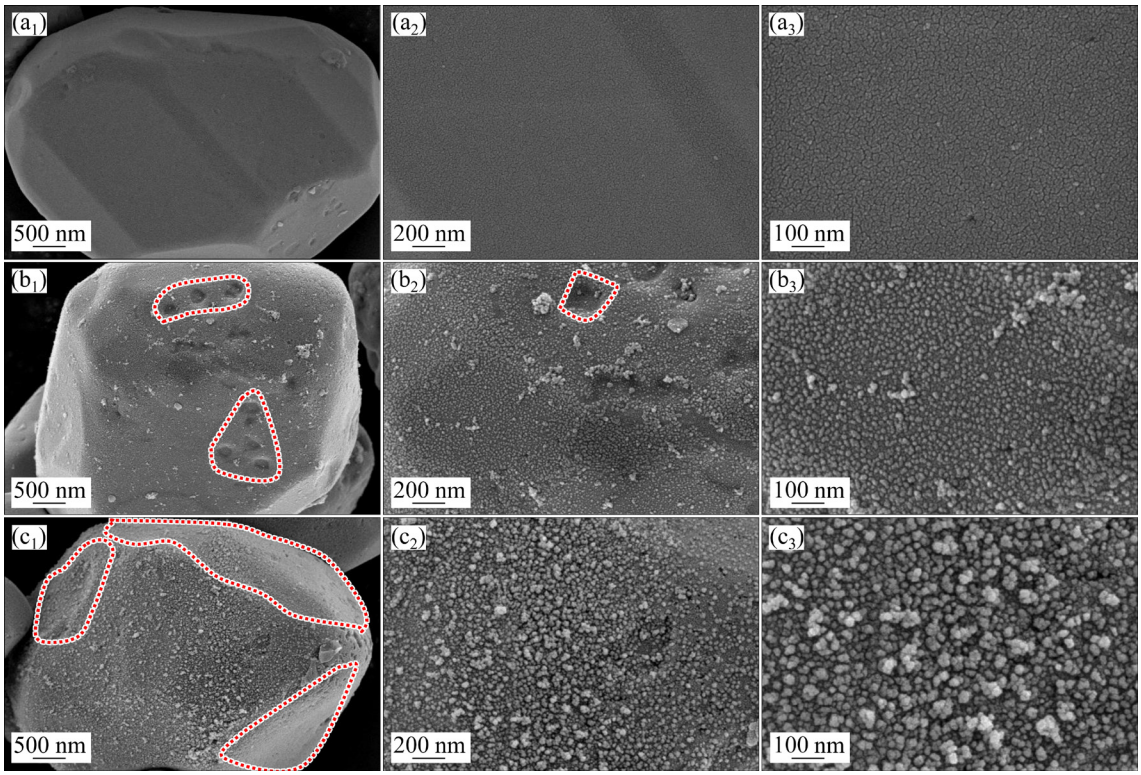

Fig. 7 FESEM images at different magnifications of anglesite particles sulfidized with different sodium sulfide solution concentrations: (a_1−a_3) Sample 1; (b_1−b_3) Sample 2; (c_1−c_3) Sample 3

PbS. Interestingly, some nanoparticles shown in Fig. 7(c_3) were cubic, which was the typical crystal morphology of galena PbS. PbS nanoparticles grown on anglesite treated with 5 mmol/L sodium sulfide solution had larger sizes than those treated with a 1.5 mmol/L sodium sulfide solution. Thus, sodium sulfide concentration may affect the size of the PbS nanoparticles.

Compared with the case without sodium sulfide, anglesite dissolution was significantly promoted in the presence of sodium sulfide. For instance, in a 1.5 mmol/L sodium sulfide solution, obvious dissolution pits, approximately rectangular, were observed in the FESEM image (marked in red in Fig. 7(b)); when sodium sulfide concentration was 5 mmol/L, although the dissolution pits might be covered by the dense PbS precipitate layer and thereby could not be observed, the anglesite particle lost its geometrically regular crystal edges (marked in red in Fig. 7(c)), probably due to the retreatment of crystal edges caused by the promoted dissolution. This promotion of anglesite dissolution may be because the formation of PbS precipitates reduces the lead concentration in the aqueous solution, leading to non-equilibrium conditions compared to that without sodium sulfide.

3.5 Sulfidization mechanism

Our results clearly demonstrated that the dissolution of $PbSO_4$ and the precipitation of PbS occurred simultaneously when anglesite was treated with sodium sulfide solutions. Thus, anglesite sulfidization can be interpreted as a result of an ICDP process that results from more than 19 orders of considerable solubility difference between PbS (K_{sp}=$10^{-27.47}$) and $PbSO_4$ (K_{sp}=$10^{-7.74}$) [13,33]. The ICDP reactions at the anglesite–sodium sulfide solution interface may be schematically illustrated in Fig. 8. The following steps are involved in anglesite sulfidization: (1) anglesite dissolution releases Pb^{2+} and SO_4^{2-} into the solution upon contact with a sodium sulfide solution; (2) the fluid boundary layer resulting from the slow diffusion of the solutes from the reaction interface to the bulk solution becomes oversaturated with respect to PbS phase; (3) PbS nucleates and grows on the surface of anglesite to generate a layer of sulfidization product. Figure 8 also presents the crystal cells of anglesite and galena, showing the microstructural difference between the sulfidization product and anglesite. The overall reaction of anglesite with a sodium sulfide solution under neutral pH conditions may be written as

$$PbSO_4(s)+HS^-(aq)\rightarrow PbS(s)+SO_4^{2-}(aq)+H^+(aq).$$

The changes in the enthalpy (ΔH) and Gibbs free energy (ΔG) of the anglesite sulfidization reaction at 0−30 °C were calculated and are listed in Table S2. Negative values of ΔH and ΔG indicate the exothermic and spontaneous nature of the sulfidization reaction. Thus, the replacement of $PbSO_4$ by PbS when anglesite is treated with a sodium sulfide solution is thermodynamically favorable under flotation-related conditions.

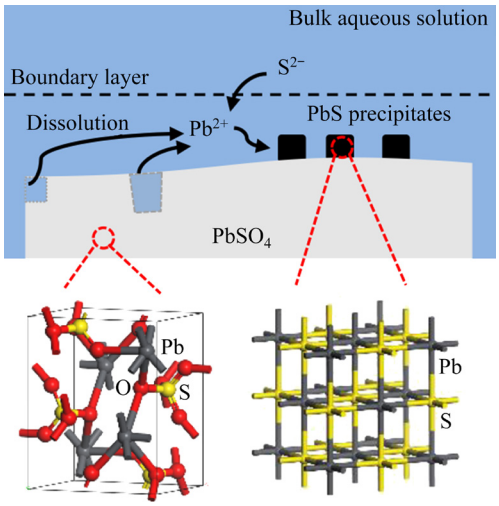

Fig. 8 Schematic illustration of anglesite sulfidization via ICDP mechanism

As well known, the moderate-concentration sulfidizing agents can promote the flotation of oxidized minerals, while excessive concentration ones can depress the flotation. As illustrated schematically in Fig. 9, the recovery versus sodium sulfide concentration plot can be divided into three parts to explain the relationship between the flotation behaviors and sulfidization states of anglesite at different sodium sulfide concentrations. Part I: under sulfide-deficient conditions, sulfide ions are completely consumed by lead ions dissolved in the bulk aqueous solution, and precipitate as PbS (labeled as $PbS_{(1)}$), that is, by a homogeneous nucleation mechanism. Part II: upon adding more sulfide ions, sulfide ions begin to diffuse to the anglesite–aqueous solution interface, and thereby induce the sulfidization of anglesite via an ICDP mechanism. With increasing the sodium sulfide concentration, both the coverage of PbS on anglesite and the flotation recovery increase until

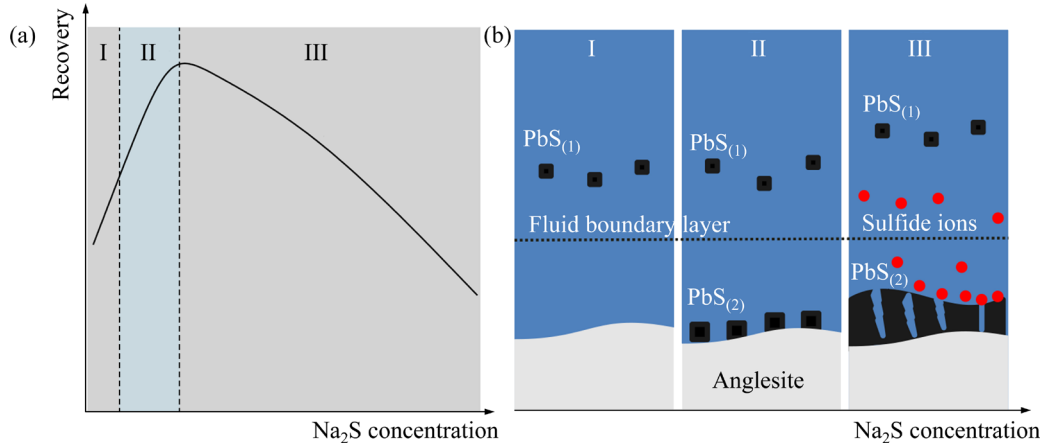

Fig. 9 Schematic illustration of flotation recovery (a) and sulfidization state (b) of anglesite at different sodium sulfide concentrations

the maximum recovery is obtained. Part III: when the sodium sulfide concentration exceeds the optimal value for flotation, the sulfidization reaction may be maintained by the formation of porosity in the product phase layer; however, a considerable part of the sulfide ions still remain in the aqueous solution due to diffusion control. The residual sulfide ions can reduce the redox potential of the pulp and cause competitive adsorption against the collector such as xanthate, thereby depressing the flotation [23].

For the conversion of $PbSO_4$ to PbS, PbS grows on $PbSO_4$ via three-dimensional heterogeneous nucleation rather than via layer-by-layer growth because they have different crystal structures; in addition, the molar volume and solubility of PbS are smaller than those of $PbSO_4$ ($V_{mol}(PbS)$= 31.48 cm^3/mol, $V_{mol}(PbSO_4)$=48.21 cm^3/mol) [34]. In this case, all the above-mentioned conditions favor the development of porosity. The porosity can be mainly attributed to the gaps between the PbS nanoparticles shown in the FESEM images at the higher magnifications (Fig. S3).

Previous studies on the sulfidization of other oxidized minerals have also presented several characteristics of an ICDP mechanism, such as the conversion of $Cu_2(OH)_2CO_3$ to $Cu_{2-x}S$ [12], $PbCO_3$ to PbS [13], and $ZnCO_3$ to ZnS [15]. In addition, the features of this mechanism are likewise reflected by the synthesis of core−shell and heterostructure materials through the interaction of metal oxides with an aqueous solution of soluble sulfides, such as the synthesis of $Cu_2O/Cu_{31}S_{16}$ [35], CuO/CuS [36], and ZnO/ZnS [37] composites. Therefore, it may be suggested that the ICDP reaction is a universal mechanism for the sulfidization of oxidized minerals or metal oxide composites when they are treated with sodium sulfide solutions.

4 Conclusions

(1) The results obtained using XPS, Raman, and UV−Vis DRS demonstrated the replacement of $PbSO_4$ by PbS during anglesite treatment with an aqueous solution of sodium sulfide. The FESEM images showed the dissolution of $PbSO_4$ as well as the precipitation of PbS during sulfidization.

(2) Anglesite sulfidization proceeds via an ICDP mechanism: upon interaction with a sodium sulfide aqueous solution, the less stable $PbSO_4$ phase dissolves while more stable PbS phase precipitates at anglesite–sodium sulfide aqueous solution interface.

(3) The PbS nanoparticle generated on anglesite, which exhibits stronger hydrophobicity and reactivity with xanthate than the $PbSO_4$ particle at sufficient sodium sulfide concentrations, is responsible for the promotion of anglesite flotation by sulfidization. However, at above the optimum sodium sulfide concentration for flotation, some sulfide ions remain in the pulp due to the limited diffusion, thereby depressing the flotation.

(4) The sulfidization flotation behavior is related to the feature of the ICDP reaction, suggesting that this mechanism has important guiding significance for the sulfidization flotation of oxidized minerals of base metals.

Acknowledgments

The authors sincerely thank the Analysis and Testing Foundation of Kunming University of Science and Technology, China (No. 2018M20162101102).

Supporting Information

Supporting Information in this paper can be found at: http://tnmsc.csu.edu.cn/download/21-p3503-2022-0463-Supporting_Information.pdf.

References

[1] PIRAJNO F, BURLOW R, HUSTON D. The Magellan Pb deposit, Western Australia: A new category within the class of supergene non-sulphide mineral systems [J]. Ore Geology Reviews, 2010, 37(2): 101−113.

[2] FAZLI S, TAGHIPOUR B, LENTZ D R. The Zn−Pb sulfide and Pb−Zn−Ag non-sulfide Kuh-e-Surmeh Ore Deposit, Zagros Belt, Iran: Geologic, mineralogical, geochemical, and S isotopic constraints [J]. Journal of Geochemical Exploration, 2018, 194: 146−166.

[3] ZHU Chuan-wei, WEN Han-jie, ZHANG Yu-xu, YIN Run-sheng, CLOQUET C. Cd isotope fractionation during sulfide mineral weathering in the Fule Zn−Pb−Cd Deposit, Yunnan Province, Southwest China [J]. Science of the Total Environment, 2018, 616/617: 64−72.

[4] HAN Hai-sheng, SUN Wei, HU Yue-hua, JIA Bao-liang, TANG Hong-hu. Anglesite and silver recovery from jarosite residues through roasting and sulfidization−flotation in zinc hydrometallurgy [J]. Journal of Hazardous Materials, 2014, 278: 49−54.

[5] YAO Wei, LI Mao-lin, CUI Rui, JIANG Xing-ke, JIANG Hong-qiang, DENG Xiao-long, LI Yun, ZHOU Sheng. Flotation behavior and mechanism of anglesite with salicyl hydroxamic acid as collector [J]. JOM, 2018, 70(12): 2813−2818.

[6] RAO Shuai, LIU Zhi-qiang, WANG Dong-xin, CAO Hong-yan, ZHU We, ZHANG Kui-fan, TAO Jin-zhang. Hydrometallurgical process for recovery of Zn, Pb, Ga and Ge from Zn refinery residues [J]. Transactions of Nonferrous Metals Society of China, 2021, 31(2): 555−564.

[7] HAN Guang, WEN Shu-ming, WANG Han, FENG Qi-cheng. Enhanced sulfidization flotation of cuprite by surface modification with hydrogen peroxide [J]. Transactions of Nonferrous Metals Society of China, 2021, 31(11): 3564−3578.

[8] MOIMANE T, PENG Yong-jun. Sulphidisation of oxides and oxidised sulphides and adsorption of thiol collectors on the sulphidised products—A critical review [J]. Advances in Colloid and Interface Science, 2022, 305: 102697.

[9] YIN Wan-zhong, SUN Qian-yu, LI Dong, TANG Yuan, FU Ya-feng, YAO Jin. Mechanism and application on sulphidizing flotation of copper oxide with combined collectors [J]. Transactions of Nonferrous Metals Society of China, 2019, 29(1): 178−185.

[10] FENG Qi-cheng, WEN SHU-ming. Formation of zinc sulfide species on smithsonite surfaces and its response to flotation performance [J]. Journal of Alloys and Compounds, 2017, 709: 602−608.

[11] FENG Qi-cheng, ZHAO Wen-juan, WEN Shu-ming, CAO Qin-bo, Copper sulfide species formed on malachite surfaces in relation to flotation [J]. Journal of Industrial and Engineering Chemistry, 2017, 48: 125−132.

[12] LIU Rui-zeng, LIU Dian-wen, LI Jia-lei, LI Jian-ming, LIU Zhi-cheng, JIA Xiao-dong, YANG Sheng-wang, LI Jiang-li, NING Shuai. Sulfidization mechanism in malachite flotation: A heterogeneous solid-liquid reaction that yields Cu_xS_y phases grown on malachite [J]. Minerals Engineering, 2020, 154: 106420.

[13] LI Jia-lei, LIU Si-yan, LIU Dian-wen, LIU Rui-zeng, LIU Zhi-cheng, JIA Xiao-dong, CHANG Tian-cang. Sulfidization mechanism in the flotation of cerussite: A heterogeneous solid−liquid reaction that yields $PbCO_3$/PbS core−shell particles [J]. Minerals Engineering, 2020, 153: 106400.

[14] LIU Rui-zeng, LIU Dian-wen, LI Jia-lei, LIU Si-yan, LIU Zhi-cheng, GAO Lian-qi, JIA Xiao-dong, AO Shun-fu. Improved understanding of the sulfidization mechanism in cerussite flotation: An XPS, ToF-SIMS and FESEM investigation [J]. Colloids and Surfaces A: Physicochemical and Engineering Aspects, 2020, 595: 124508.

[15] LIU Rui-zeng, PEI Bin, LIU Zhi-cheng, WANG Yun-wei, LI Jia-lei, LIU Dian-wen. Improved understanding of the sulfidization mechanism in amine flotation of smithsonite: An XPS, AFM and UV−Vis DRS study [J]. Minerals, 2020, 10(4): 370.

[16] LUO Bin, LIU Quan-jun, DENG Jiu-shua, YU Li, LAI Hao, SONG Chao, LI Shi-mei. Characterization of sulfide film on smithsonite surface during sulfidation processing and its response to flotation performance [J]. Powder Technology, 2019, 351: 144−152.

[17] DENG Jiu-shuai, LAI Hao, WEN Shu-ming, LI Shi-mei. Confirmation of interlayer sulfidization of malachite by ToF-SIMS and principal component analysis [J]. Minerals, 2019, 9(4): 204.

[18] WANG Li-jun, PUTNIS C V. Dissolution and precipitation dynamics at environmental mineral interfaces imaged by in situ atomic force microscopy [J]. Accounts of Chemical Research, 2020, 53(6): 1196−1205.

[19] RUIZ-AGUDO E, PUTNIS C V, PUTNIS A. Coupled dissolution and precipitation at mineral–fluid interfaces [J]. Chemical Geology, 2014, 383: 132−146.

[20] PUTNIS A, PUTNIS C V. The mechanism of reequilibration of solids in the presence of a fluid phase [J]. Journal of Solid State Chemistry, 2007, 180(5): 1783−1786.

[21] RENARD F, RØYNE A, PUTNIS C V. Timescales of interface-coupled dissolution−precipitation reactions on carbonates [J]. Geoscience Frontiers, 2019, 10(1): 17−27.

[22] RASHCHI F, DASHTI A, ARABPOUR-YAZDI M, ABDIZADEH H. Anglesite flotation: A study for lead recovery from zinc leach residue [J]. Minerals Engineering, 2005, 18(2): 205−212.

[23] TANG Hong-hu, JIANG Feng, HU Yue-hua, HAN Hai-sheng, WANG Li, SUN Wei. Flotability of laurionite

and its response to sulfidization flotation [J]. Minerals Engineering, 2020, 148: 106183.
[24] ELIZONDO-ÁLVAREZ M A, URIBE-SALAS A, NAVA-ALONSO F. Flotation studies of galena (PbS), cerussite ($PbCO_3$) and anglesite ($PbSO_4$) with hydroxamic acids as collectors[J]. Minerals Engineering, 2020, 155: 106456.
[25] ZHANG Qian, WEN Shu-ming, FENG Qi-cheng, ZHANG Song. Surface characterization of azurite modified with sodium sulfide and its response to flotation mechanism [J]. Separation and Purification Technology, 2020, 242: 116760.
[26] JIA Xiao-dong, SONG Kai-we, CAI Jin-peng, SU Chao, XU Xiao-hui, MA Yin-yu, SHEN Pei-lun, LIU Dian-wen. Effect of oxygen and sodium sulfide on the flotation of cuprite and its modification mechanism [J]. Transactions of Nonferrous Metals Society of China, 2023, 33: 1233−1243.
[27] NIST X-ray Photoelectron spectroscopy database [EB/OL]. [2022−09−05]. https://srdata.nist.gov/xps/.
[28] FAN Feng-tao, XU Qian, XIA Hai-an, SUN Ke-ju, FENG Zhao-chi, LI Can. UV Raman spectroscopic characterization of catalytic materials [J]. Chinese Journal of Catalysis, 2009. 30(8): 717−739. (in Chinese)
[29] VISCARRA ROSSEL R A, MCGLYNN R N, MCBRATNEY A B. Determining the composition of mineral-organic mixes using UV−Vis−NIR diffuse reflectance spectroscopy [J]. Geoderma, 2006, 137(1/2): 70−82.
[30] HAN Bin, XIE An-jian, YU Qing-bo, HUANG Fang-zhi, SHEN Yu-hua, ZHU Ling. Synthesis of $PbSO_4$ crystals by hydrogel template on postprocessing strategy for secondary pollution [J]. Applied Surface Science, 2012, 261: 623−627.
[31] JEHLIČKA J, VÍTEK P, EDWARDS H G M, HEAGRAVES M, ČAPOUN T. Application of portable Raman instruments for fast and non-destructive detection of minerals on outcrops [J]. Spectrochimica Acta, 2009, 73(3): 410−419.
[32] MERNAGH T P, TRUDU A G, A laser Raman microprobe study of some geologically important sulphide minerals [J]. Chemical Geology, 1993, 10 (1/2/3/4): 113−127.
[33] NIKKHOU F, XIA F, KNORSCH M, DEDITIUS A P. Mechanisms of surface passivation during galena leaching by hydrogen peroxide in acetate and citrate solutions at 25−50 °C [J]. ACS Sustainable Chemistry & Engineering, 2020, 8: 14407−14416.
[34] YUAN K, DE ANDRADE V, FENG Z G, STURCHIO N C, LEE S S, FENTER P. Pb^{2+}–calcite interactions under far-from-equilibrium conditions: formation of micropyramids and pseudomorphic growth of cerussite [J]. The Journal of Physical Chemistry C, 2018, 122(4): 2238−2247.
[35] LIU Xue-qin, LI Zhen, ZHANG Qiang, LI Fei. Controllable synthesis and enhanced photocatalytic properties of Cu_2O/$Cu_{31}S_{16}$ composites [J]. Materials Research Bulletin, 2012, 47(9): 2631−2637.
[36] LI Dong, HE Yong-jun, WANG Sha. On the rotation of the Janus CuO/CuS Colloids formed at a Pickering emulsion interface [J]. The Journal of Physical Chemistry C, 2009, 113(30): 12927−12929.
[37] REN Ze-qian, LI Xiu, GUO Li-xia, WU Ji-zhou, LI Yu-qing, LIU Wen-liang, LI Peng, FU Yong-ming, MA Jie. Facile synthesis of ZnO/ZnS heterojunction nanoarrays for enhanced piezo-photocatalytic performance [J]. Materials Letters, 2021, 292: 129635.

界面耦合的 $PbSO_4$ 溶解和 PbS 沉淀及其对铅矾硫化浮选的影响

李佳磊[1]，李广利[2]，刘志成[2]，宁 帅[1,3]，刘瑞增[1,3]

1. 昆明理工大学 国土资源工程学院，昆明 650093；
2. 云南驰宏锌锗股份有限公司，曲靖 655000；
3. 云南省战略金属矿产资源绿色分离与富集重点实验室，昆明 650093

摘 要：通过浮选试验、X 射线光电子能谱(XPS)、场发射扫描电子显微镜(FESEM)、拉曼光谱和紫外−可见漫反射光谱(UV−Vis DRS)系统研究铅矾浮选中的硫化机理。浮选试验证明硫化钠对铅矾浮选具有活化作用；但必须控制硫化钠浓度，以避免过量硫离子对浮选的抑制。XPS、拉曼光谱和 UV−Vis DRS 结果表明，用硫化钠水溶液处理铅矾时，$PbSO_4$ 被 PbS 取代。FESEM 观察结果显示硫化过程中 $PbSO_4$ 的溶解和 PbS 纳米粒子的沉淀。因此，可认为铅矾与硫化钠水溶液的反应是通过界面耦合溶解–沉淀机制进行的：在与硫化钠水溶液接触时，铅矾溶解将 Pb^{2+}和 SO_4^{2-}释放到流体边界层中，该流体边界层相对于 PbS 相变得过饱和；然后，PbS 纳米粒子在铅矾表面成核并生长。生长在铅矾表面的 PbS 纳米颗粒可以提高铅矾的可浮性。

关键词：铅矾；硫酸铅；硫化铅；硫化机理；浮选；溶解；沉淀

(Edited by Wei-ping CHEN)